RESEARCH ARTICLE | JULY 07 2025

Micro-engineered Cu–Ag catalysts as analytical tools for direct observation of hetero-interfaces and surface structures

Ryo Hishinuma ; Hiroya Tanaka ; Keita Funayama

AIP Advances 15, 075111 (2025)
https://doi.org/10.1063/5.0271594

Micro-engineered Cu–Ag catalysts as analytical tools for direct observation of hetero-interfaces and surface structures

Cite as: AIP Advances 15, 075111 (2025); doi: 10.1063/5.0271594
Submitted: 5 June 2025 • Accepted: 14 June 2025 •
Published Online: 7 July 2025

Ryo Hishinuma,[a] Hiroya Tanaka, and Keita Funayama[b]

AFFILIATIONS

Toyota Central R&D Labs., Inc., Nagakute 480-1192, Japan

[a]Author to whom correspondence should be addressed: r-hishinuma@mosk.tytlabs.co.jp
[b]Electronic mail: funayama@mosk.tytlabs.co.jp

ABSTRACT

The development of technologies for analyzing electrochemical catalysts is crucial for improving catalytic performances, including productivity and product selectivity. However, in conventional composite catalysts, directly observing local reaction sites and structures is challenging due to the size and random positioning of nanoparticles. In this study, we investigated hetero-interfacial reaction sites and surface structures before and after the electrochemical CO_2 reduction reaction using a micropatterned Cu–Ag catalyst. The scalable catalyst design enabled direct analysis of oxygen adsorption on the Cu surface near the Cu–Ag hetero-interface following the electrochemical reduction reaction. The artificial flatness of the patterned catalyst also allowed for the quantitative evaluation of surface roughness changes on Cu and Ag, corresponding to the nanoparticle surfaces of composite catalysts. Furthermore, we demonstrated the potential for reaction product selectivity by microengineering the length of local reaction sites, such as the Cu–Ag hetero-interface. Our platform provides a valuable analytical toolset and framework for revealing catalytic reaction phenomena and enhancing catalytic performance.

I. INTRODUCTION

The electrochemical carbon dioxide reduction reaction (CO_2RR) has garnered significant interest for recycling carbon dioxide as an energy source under ambient temperatures and pressures.[1–7] Catalysts play a crucial role in enhancing the conversion efficiency of the CO_2RR to hydrocarbon and alcohol products, such as ethylene, methane, and ethanol.[8–12] In the conversion of CO_2 into value-added chemicals, the progression of multiple reactions in multicomponent catalysts mutually supports each reaction step. In particular, the local reaction sites around the hetero-interface in such catalysts have been considered influential in catalytic activity; consequently, reaction mechanisms have recently been studied using various composite catalysts.[13–20] However, the changes in local reaction sites and catalytic structures induced by electrochemical reactions remain insufficiently understood. This is because in conventional composite catalyst fabrication processes, the local reaction sites and micro-/nano-structures cannot be accurately and arbitrarily designed. Such uncontrollable characteristics prevent direct observation of hetero-interfaces and tiny areas such as nanoparticle surfaces.[21–26]

Microfabrication technology has great potential to address these issues because it enables the artificial production of miniature structures on the micrometer scale and smaller. Recent literature has increasingly highlighted phenomena at the hetero-interface using microfabrication technology.[27–33] For example, Lum and Ager demonstrated that micropatterned Cu catalysis allows control of the ratio of oxygenates to ethylene by tuning the distance between Cu- and CO-producing catalysts in aqueous CO_2 reduction.[27] Similarly, Larrazábal *et al.* showed that the high CO evolution activity of Cu–In catalysts is associated with indium-poor bimetallic phases formed under reaction conditions near Cu–In interfaces.[28] Dong *et al.* investigated the effect of grain boundary oxidation in Cu–Ag thin films on the selectivity of CO and CH_4 production. They found that Cu thin films with smaller grain sizes are susceptible to spontaneous oxidation, which degrades the Faradaic efficiency of production.[29]

However, further investigations are required to fully understand the mechanisms of electrochemical reduction reactions and the structural changes at hetero-interfaces.

In the present study, we investigated the changes in the hetero-interfacial reaction sites and surface structures of Cu–Ag catalysts before and after electrochemical CO_2RR. We prepared micropatterned Cu–Ag catalysts consisting of periodic Ag square arrays on single-crystal Cu substrates using microfabrication technologies such as photolithography. These artificially patterned catalysts enabled the quantitative evaluation of changes in catalyst surfaces and reaction sites during CO_2RR. Local analysis using energy-dispersive x-ray spectroscopy (EDS) directly revealed increased oxygen adsorption on the Cu surface near the Cu–Ag hetero-interface after CO_2RR. In addition, unlike nanoparticle surfaces, the scalability and flatness of the micropatterned catalysts allowed quantitative evaluation of the mean and variance of surface roughness on Cu and Ag using atomic force microscopy (AFM) before and after the reaction. Our approach provides a tool for capturing detailed catalyst properties, thereby facilitating a better understanding of the CO_2RR mechanism at hetero-interfaces.

II. MATERIALS AND METHODS

A. Preparation of the micro-pattered Cu–Ag catalyst

We studied the variation in the hetero-interfacial and structural characteristics of a Cu–Ag-based catalyst before and after electrochemical reactions using a micropatterned catalyst instead of a conventional composite catalyst. Figure 1 shows schematics of a conventional composite catalyst (left panel) and a micropatterned catalyst (right panel) consisting of two types of catalytic materials (catalysts 1 and 2). In composite catalysts, randomly scattered nanoparticles prevent us from analyzing their structural characteristics, such as surface roughness, and observing local reaction sites, such as hetero-interfaces. On the other hand, microfabrication technology enables us to artificially design the position and scale of the reaction sites by controlling the structural parameters, for example, the side length w of the square patterns, pattern spacing D, and hetero-interface length L, as shown in Fig. 1. In this study, we fabricated Ag periodic square patterns on a Cu(100) substrate using a microfabrication technology that is familiar with semiconductor device fabrication.

The steps for the fabrication of the micropatterned Cu–Ag catalyst are summarized in Fig. 2(a). We prepared a Cu substrate with a plane orientation of (100) (Shanghai Institute of Optics and Fine Mechanics, Chinese Academy of Sciences), which is $15 \times 25 \times 0.5t$ mm. The Cu substrate was cleaned using acetone, isopropyl alcohol (IPA), and deionized (DI) water with ultrasonic cleaning for 5 min each [Fig. 2(a-i)]. Using photolithography, we drew a pattern of a periodic Ag square array on a Cu substrate [Fig. 2(a-ii)]. To enhance the adhesion between the substrate and the photoresist, hexamethyldisilazane (Tokyo Ohka Kogyo Co. Ltd., OAP) was spin-coated onto the substrate at 5000 rpm for 50 s. Subsequently, a photoresist (Tokyo Ohka Kogyo Co. Ltd., THMR-iP3100 MM) was spin-coated under the same conditions as the OAP and pre-baked at 90 °C for 90 s. The substrate was inserted into a mask aligner (EV Group, EVG620) and patterned by illuminating ultraviolet light in contact with the photomask. After lithography, we dipped the substrate in the developer (Tokyo Ohka Kogyo Co. Ltd., NMD-W 2.38%) for 3 min and rinsed it with DI water for 1 min. We obtained a substrate with a resist pattern by post-baking at 110 °C for 90 s. Using electron beam evaporation equipment (Canon Anelva Corporation, EVD-500B), a Ag thin film with a thickness of 50 nm was fabricated on a substrate with a resist pattern at a pressure of 1.8×10^{-4} Pa and a deposition rate of 0.2 nm/s [Fig. 2(a-iii)]. A lift-off process was then used to remove the Ag from the Cu substrate, with the photoresist in the remover for 24 h. After ultrasonic cleaning in acetone, IPA, and DI water for 5 min each, we obtained a complete Cu–Ag catalyst with a pattern consisting of periodic Ag squares on the Cu substrate [Fig. 2(a-iv)]. Figure 2(b) shows a microscopic image of the fabricated catalyst with (w, D) = (20 μm, 40 μm). A 20×10 mm^2 patterned area on the Cu–Ag catalyst was used for the CO_2RR.

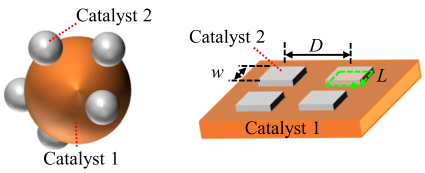

FIG. 1. Schematics of a conventional composite catalyst and micro-/nano-patterned catalyst consisting of two catalyst materials. The distance between periodic patterns D, side length of the square-shaped pattern w, and hetero-interface length L are examples of artificially controllable parameters by micro-/nano-fabrication technology.

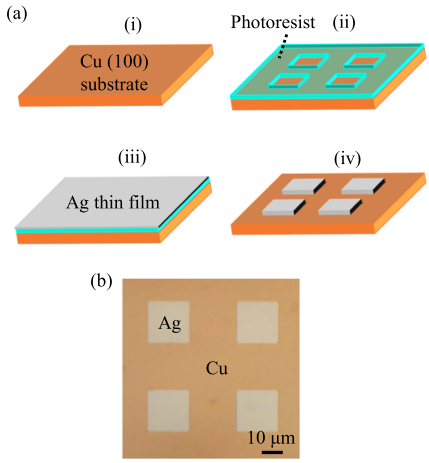

FIG. 2. (a) Schematics of fabrication process for Cu–Ag micropatterned catalyst. The fabrication step is in the order of (i) to (iv). (b) Microscopic image of the completed micropatterned Ag squares with (D, w) = (40 μm, 20 μm) on a Cu(100) substrate. Here, D and w represent the periodic distance and side length of the square-shaped Ag pattern, respectively, as shown in Fig. 1.

B. Characterization

We used a scanning electron microscope (SEM) (Hitachi High-Tech Corporation, S-4800) to observe the surface of the patterned catalyst before and after CO_2RR. We observed the catalyst, which was allowed to electrochemically react for 1 h under each of five voltage conditions, i.e., a total of 5 h, as the sample of post-CO_2RR.

We also conducted EDS (Oxford Instruments, UltimMax65) to investigate the elemental distributions on the surface and hetero-interface of the patterned catalyst. Ag and Cu surface conditions were analyzed by AFM (Hitachi High-Tech Corporation, E-sweep). Crystallinity of the Cu substrate and the deposited Ag film was analyzed using x-ray diffraction (XRD) (Rigaku Holdings Corporation, RINT-TTR).

C. Electrochemical measurement and product analysis

Electrochemical measurements were conducted in an original H-type cell separated using a bipolar membrane (Fumatech GmbH, Fumasep FBM) with a three-electrode system with a potentiostat/galvanostat (Meiden Hokuto Corp., HZ-Pro). The bipolar membrane prevents the alcohol products such as C_2H_5OH and C_3H_7OH from crossing over to the anode, as shown in the literature.[34,35] An Ag/AgCl reference electrode (EC Frontier Co. Ltd., RE-11A) was inserted between the fabricated Cu–Ag catalyst and the bipolar membrane, and the counter electrode was a Pt mesh. The electrolyte used for these measurements was 0.1M $KHCO_3$. CO_2 gas was directly introduced into the electrolyte solution from near the patterned catalyst during the CO_2RR. As a preparation of CO_2RR, CO_2 bubbling to the electrolyte was carried out for 30 min before electrochemical reaction, similar to the literature.[27–29] The applied reversible hydrogen electrode [V_{RHE} (V)] was calculated from the potential in the cell ($V_{Ag/AgCl}$) (V) by the Nernst equation considering the potential drop due to the resistance in our cell, i.e., $V_{RHE} = V_{Ag/AgCl} + 0.2 + 0.059 \times pH + I_{Ave}R$. Here, I_{Ave} is the average measured current and R is the resistance obtained from the impedance measurement. Note that the macroscopic position of Cu and Ag and flow direction of raw material such as CO_2 become significant parameters under high current density,[36] while the effect of them is negligible small under low current density.[31–33]

The gas products produced by CO_2RR were analyzed using a gas chromatograph (SRI Instruments, 8610C). The liquid products were analyzed using a gas chromatograph equipped with a headspace sampler (Agilent Technologies Inc., 7890A). All measurements were performed under ambient conditions and at room temperature.

III. RESULTS AND DISCUSSION

A. Direct observation of hetero-interface

The micropatterned catalyst has great potential as a platform to analyze the variance in local reaction sites via electrochemical reactions. We evaluated the Cu–Ag hetero-interface before and after CO_2RR using a micropatterned catalyst.

We confirmed that the micropattern functioned as a catalyst for the CO_2RR. Figures 3(a) and 3(b) show the measured total current I_{to} and Faradaic efficiency, respectively, as functions of the applied potential V_{RHE} using the patterned catalyst. Electrochemical measurements with the micropatterned catalyst produced hydrocarbons and alcohols, in addition to hydrogen, while there is unresolved future work that the reason why methane is a dominant product, such as the case for Cu(111).[24,37] Ag (Cu) decomposes CO_2 (CO) to produce CO (hydrocarbons and alcohols).[7,38–46] Thus, the obtained products indicate that a series of reduction reactions from CO_2 to

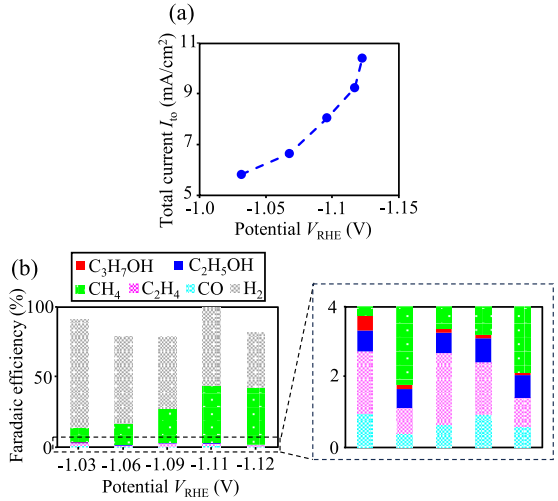

FIG. 3. (a) Total current I_{to} as a function of applied potential V_{RHE}. (b) Faradaic efficiencies for the five different potential conditions. The right panel shows the enlarged view of the left panel in the range of the FEs from 0% to 4%.

hydrocarbons and alcohols occurred on the micropatterned Cu–Ag catalyst, similar to the reactions on conventional Cu–Ag composite catalysts. These results confirm that the micropattern functioned as a CO_2-reduction catalyst. Considering from the Faradaic efficiency, there may be undetected products due to the insufficient resolution of the instrument or incompatible products for the instrument. However, such minor and small amounts of products are outside the scope of this study. Note that CO_2 and OH^- mass transfer is one of the factors affecting the reaction products under relatively high current density, e.g., >100 mA/cm^2.[36] On the other hand, for low current density, the effect of mass transport is conventionally small enough to be ignored.

Using SEM-EDS observations, we evaluated the elemental distributions on the catalyst for pre- and post-CO_2RR. First, the elemental distribution of the patterned catalyst was macroscopically observed. Figures 4(a)–4(e) [Figs. 4(f)–4(j)] show SEM images and elemental maps of Cu, Ag, C, and O, respectively, before (after) CO_2RR. The elemental distribution of Cu [Figs. 4(b) and 4(g)] and Ag [Figs. 4(c) and 4(h)] indicates that the patterned structures remained without drastic changes, such as losses and deformations through CO_2RR. Carbon [Figs. 4(d) and 4(i)] and oxygen [Figs. 4(e) and 4(j)] were preferentially adsorbed on Cu and Ag, respectively, regardless of CO_2RR.

Second, for the microscopic analysis of the local reaction sites, we conducted a one-dimensional (1D) EDS analysis around the Cu–Ag hetero-interface. Figure 4(k) shows the SEM image of the hetero-interface before CO_2RR and a scanning line colored by magenta. Transitions in the elemental distributions of Cu (blue) and Ag (red) [Fig. 4(l)] clearly capture the existence of a hetero-interface. Oxygen (green) and carbon (cyan) are predominantly detected on Cu and Ag, respectively, similar to the macroscopic maps shown in Figs. 4(d) and 4(e). Figures 4(m) and 4(n) show the SEM images around the hetero-interface and the elemental distributions along the magenta colored scanning line after CO_2RR, respectively. The

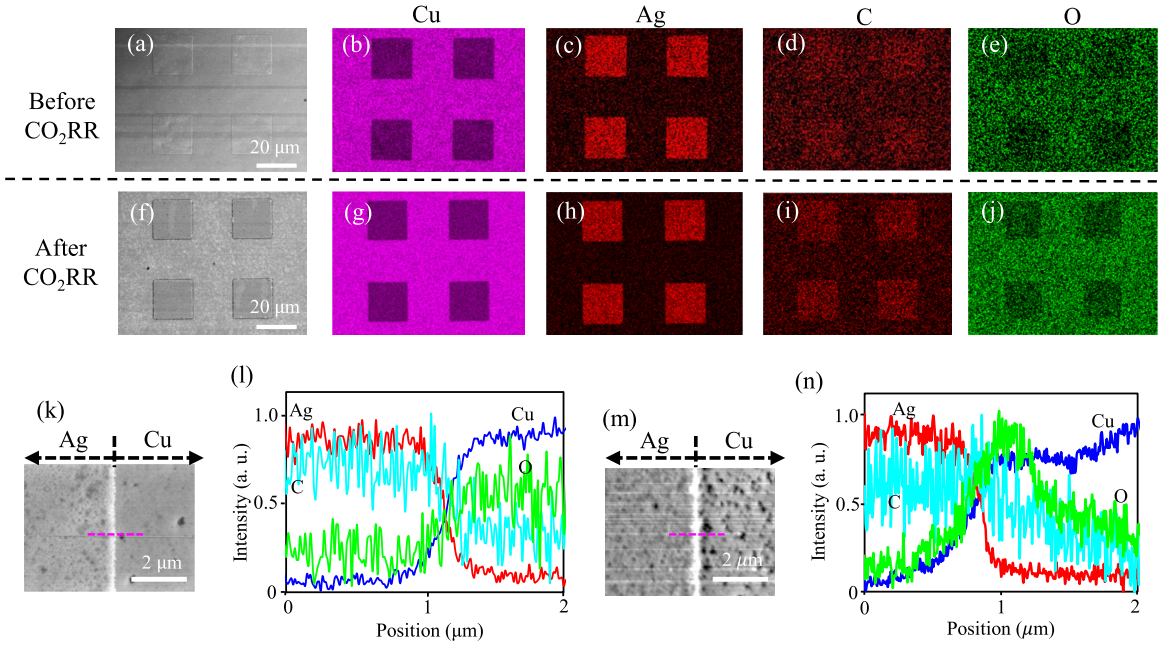

FIG. 4. (a)–(j) Top-views of SEM images [(a) and (b)] and elemental mappings for Cu [(b) and (g)], Ag [(c) and (h)], C [(d) and (i)], and O [(e) and (j)] before and after CO_2RR. (k)–(n) Top-views of SEM images around hetero-interface between Ag and Cu [(k) and (m)], and one-dimensional elemental distributions along the magenta lines [(l) and (n)] before and after CO_2RR.

results for Cu, Ag, and C are similar to those in Fig. 4(l). On the other hand, interestingly, we see that the oxygen profile for post-reaction has a peak on the local Cu region neighboring the hetero-interface. Thus, the micropatterned catalyst enabled us to directly observe oxygen adsorption near the hetero-interface. Indeed, an increase in the number of remaining Cu–O bonds after the reaction has been reported by introducing Cu–Ag hetero-interfaces in Cu-based catalysts, resulting in the promotion of hydrocarbon and alcohol production.[39,47] Our corresponding results strongly indicate that the number of remaining Cu–O bonds dominantly increased near the Cu–Ag hetero-interface. Therefore, the micropatterned catalyst is a useful platform for directly observing changes in local reaction sites before and after electrochemical reactions.

B. Quantification of catalytic surface structure

The scalability of the patterned catalysts allows us to easily design flat and large catalytic material surfaces that are normally difficult to prepare for nanoparticle-based composite catalysts. Taking advantage of these artificial structures, we evaluated the surface roughness of Ag and Cu before and after the reaction using AFM. Such structural information, alongside material composition, is crucial for understanding the mechanism of catalytic reactions.

Figures 5(a) and 5(b) present AFM images of an Ag pattern and a Cu surface, taken before and after CO_2RR, respectively. Our analysis revealed that the Ag square pattern remained intact, showing no significant signs of reaction or degradation. To further investigate the surface condition, we plotted the 1D-height profiles along the cyan lines from p to p′ in Figs. 5(a) and 5(b). The solid black (red) lines in Fig. 5(c) show the height (h) profile for pre- (post-) reaction. This AFM analysis indicated that CO_2RR induced an increase in the surface roughness of Cu and Ag and a decrease in the height h of the Ag. Because of the flatness of the patterned catalyst, we quantitatively evaluated its surface structure. In particular, we calculated the averages and variances of the heights of the Cu and Ag surfaces before and after the CO_2RR from the height profiles. The right panel in Fig. 5(c) shows the visualized surface information expressed as a probability density function $p(h)$, i.e., $p(h) = (1/\sqrt{2\pi\sigma^2}) \exp[-(h-\mu)^2/2\sigma^2]$. Here, μ and σ^2 denote the average and variance of the height profiles, respectively. The dashed and dotted gray (magenta) lines in Fig. 5(c) show the average heights of Cu(= 4.44 nm) [(= 8.27 nm)] and Ag(= 58.27 nm) [(= 48.89 nm)] before (after) CO_2RR. Compared with the profile before CO_2RR, the Ag height from the Cu surface decreased by 24.5% after CO_2RR. The variance σ^2 calculated from the profile indicates the degree of surface roughness. The height variance on Ag (Cu) surface increases from $\sigma^2 = 2.28$ nm^2 (5.97 nm^2) to $\sigma^2 = 32.1$ nm^2 (23.4 nm^2) following CO_2RR. This result contributes to providing a preferable particle size by considering the increase in surface roughness by CO_2RR.

In addition to the surface roughness, the crystallinity of Cu and Ag was investigated. Figure 5(d) shows the XRD spectra of the patterned catalyst before (black line) and after (red line) CO_2RR. In the left panel, the spectra having peaks corresponding to Cu(200) ensure that the Cu substrate maintains single crystallinity for both pre- and post-CO_2RR. The right panel indicates the enlarged spectra around

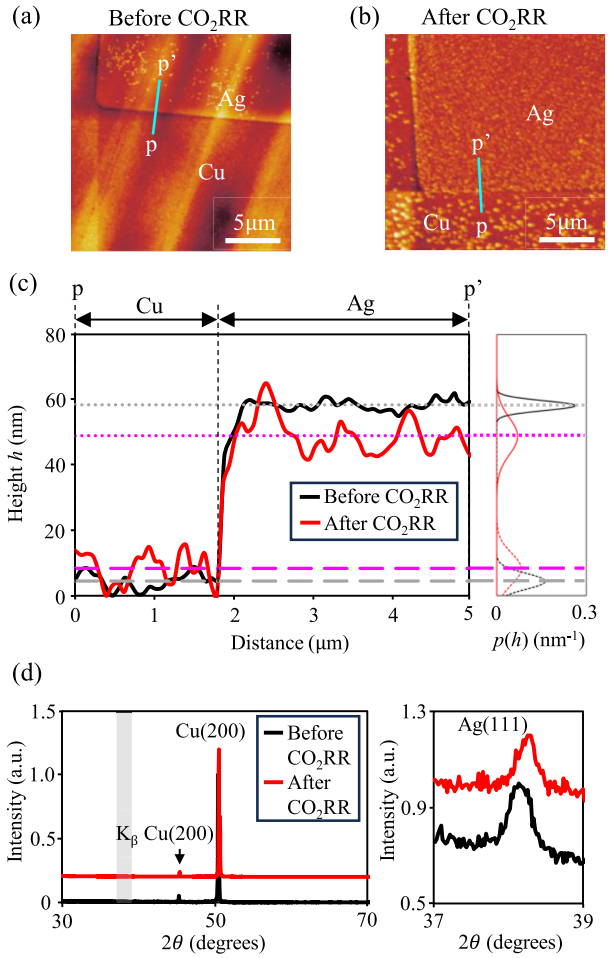

FIG. 5. (a) and (b) AFM images before (a) and after (b) CO_2RR. (c) One dimensional height profiles along the cyan line from p to p′ in (a) and (b), and probability density distributions $p(h)$ of height h. The black (magenta)-broken and -dashed lines represent the average height of Cu and Ag surfaces before (after) CO_2RR. (d) X-ray diffraction patterns of the micropatterned Cu–Ag catalyst before (black) and after (red) CO_2RR. The left panel shows the spectra in a wide range of 2θ from 30° to 70°. The right panel indicates the enlarged spectra in the range of the gray shaded region in the left panel.

the peak of Ag(111), which is in the gray shaded region in the left panel. Compared with the two spectra, we see that the crystallinity does not deteriorate because of CO_2RR regardless of the increase in the surface roughness. Note that a slight peak shift was guessed to occur due to flatness distortion induced by fixing the substrate during the electrochemical measurements because all the observed peaks [Cu(200), K_β Cu(200), and Ag(111)] similarly shifted 0.1° to the lower angle side.

Therefore, the platform enables us to quantitatively analyze changes in the catalytic structure, such as surface roughness, for which it has been difficult to obtain sufficiently flat and large surface areas for direct observation using conventional composite catalysts.

C. Selectivity of reaction products by controlling the structural parameters in micropattern

The results in the previous sections clearly show that the hetero-interface between Cu and Ag contributes to CO_2RR. To further show the evidence of the catalytic function on the hetero-interface, we investigate the dependence of the length of hetero-interface on the ratio of reaction products. Microengineering technology has the potential to control reaction activity by accurately and arbitrarily designing structural parameters such as the hetero-interface. In this study, we prepared two micropatterned electrodes with (D, w) = (40 μm, 20 μm) and (5.7 μm, 2.875 μm) to compare their electrochemical CO_2RR performance. Figure 6(a) shows the SEM image of the micropatterned electrode with (D, w) = (5.7 μm, 2.875 μm).

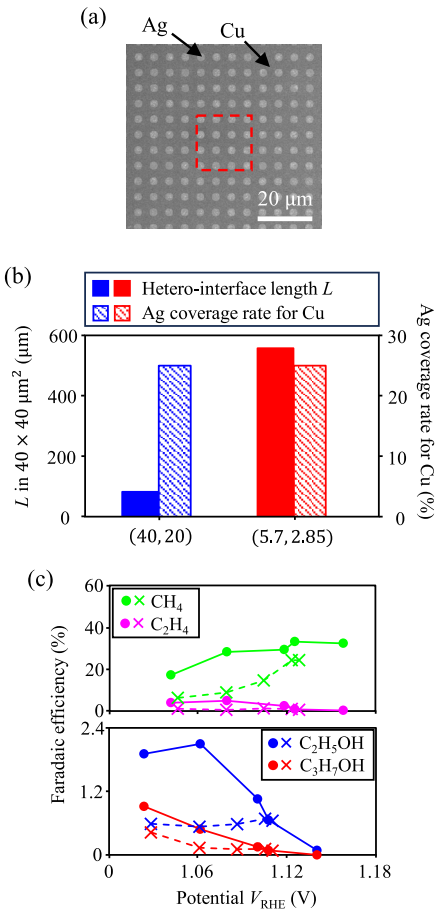

FIG. 6. (a) Top-view SEM image of the periodic Ag pattern with (D, w) = (5.7 μm, 2.85 μm) on the Cu(100) substrate. The dashed red square represents the size of one Ag pattern of (D, w) = (40 μm, 20 μm), as shown in Figs. 2 and 4. (b) Total hetero-boundary length L in the area on 40 × 40 $μm^2$ square (solid bars) and Ag coverage rate for Cu (shaded bars). The blue and red colored bars represent the patterned catalysts with (D, w) = (40 μm, 20 μm) and (5.7 μm, 2.85 μm), respectively. (c) Faradaic efficiencies of the pattered catalysts with (D, w) = (40 μm, 20 μm) (cross symbols) and (5.7 μm, 2.85 μm) (circle symbols). The green, magenta, blue, and red plots indicate Faradic efficiencies for CH_4, C_2H_4, C_2H_5OH, and C_3H_7OH, respectively.

The red squares in Fig. 6(a) show the size of one Ag square for the catalyst, where (D, w) = (40 μm, 20 μm). Figure 6(b) shows the Cu–Ag hetero-interface length L and the Ag coverage rate for Cu for each catalyst in an area of 40 × 40 μm^2. The flexible designability of microengineering technology allowed us to tune L while maintaining a constant coverage rate for the two catalysts. Thus, we evaluated the effect of the Cu–Ag hetero-interface as a local reaction site for electrochemical reduction reaction products. Figure 6(c) shows the Faradaic efficiency of all multielectron reduction ($>2e^-$) products, i.e., CH_4 (green), C_2H_4 (magenta), C_2H_5OH (blue), and C_3H_7OH (red), as a function of V_{RHE}. The circles and crosses represent the results for micropatterned Cu–Ag catalysts with (D, w) = (40 μm, 20 μm) and (5.7 μm, 2.875 μm), respectively. The micropatterned catalyst with a longer hetero-interface showed a higher Faradaic efficiency for all products than that with a shorter hetero-interface. Through the demonstration in terms of the ratio of reaction products, the reliability of the analysis of the hetero-interface is enhanced. In addition, referring to the literature,[16,18,39,47] the obtained result is reasonable because the Cu–Ag hetero-interface satisfies the conditions as a favorable local reaction site for multistep reduction reaction from CO_2 to multielectron reduction products through CO. First, CO is formed on the Ag surface from CO_2. Then, around the hetero-interface, CO can quickly reach the Cu surface for further reduction, resulting in multielectron reduction products. Therefore, accurately controllable microengineering technology has great potential for designing local reaction sites for the selectivity of each desired product.

IV. CONCLUSION

In this work, we analyzed changes in the hetero-interface and surface state before and after electrochemical CO_2RR using a micropatterned Cu–Ag catalyst. The micropattern successfully functioned as a CO_2-reduction catalyst, producing hydrocarbons and alcohols. The finely controllable scalability and position of the pattern enabled direct and straightforward observation of changes in elemental distributions around the Cu–Ag hetero-interfaces through CO_2RR. After CO_2RR, oxygen adsorption on the Cu surface increased locally near the Cu–Ag hetero-interface. This finding strongly supports the theory that the hetero-interface facilitates oxygen supply and enhances local electrochemical reaction sites for producing hydrocarbons and alcohols from CO_2. In addition, we observed the surface roughness of the Cu–Ag catalyst, which is conventionally difficult to quantitatively analyze using composite catalysts due to the size and non-flatness of nanoparticles. The flatness and scalability of the micropatterned catalyst enabled the evaluation of average heights and variances of the Cu and Ag surfaces. CO_2RR induced a 24.5% decrease in the height of the Ag patterns and an increase in the variance of the Ag (Cu) surface roughness by 14.1 (3.9) times. Quantifying such structural information is critical for understanding catalyst degradation mechanisms. Finally, as a demonstration of the future potential of our platform, we investigated the selectivity of reaction products by controlling the structural parameters. The Faradaic efficiencies of hydrocarbons and alcohols increased with the length of the Cu–Ag hetero-interface, without altering the Ag coverage of Cu. This flexible designability through microengineering is valuable for identifying and observing local reaction sites, enhancing specific electrochemical reactions, and optimizing the spatial design and composition of catalytic materials. We hope that this work will contribute to the development of an effective analytical tool and framework for understanding catalytic performance, paving the way for advancements in catalyst design and application.

AUTHOR DECLARATIONS

Conflict of Interest

The authors have no conflicts to disclose.

Author Contributions

Ryo Hishinuma: Conceptualization (lead); Data curation (lead); Formal analysis (lead); Investigation (lead); Methodology (lead); Supervision (lead); Validation (lead); Visualization (lead); Writing – original draft (lead); Writing – review & editing (lead). **Hiroya Tanaka**: Investigation (equal); Resources (lead); Supervision (lead). **Keita Funayama**: Conceptualization (lead); Data curation (lead); Formal analysis (lead); Investigation (lead); Methodology (lead); Supervision (lead); Validation (lead); Visualization (lead); Writing – original draft (lead); Writing – review & editing (lead).

DATA AVAILABILITY

The data that support the findings of this study are available from the corresponding author upon reasonable request.

REFERENCES

[1] S. Nitopi, E. Bertheussen, S. B. Scott, X. Liu, A. K. Engstfeld, S. Horch, B. Seger, I. E. L. Stephens, K. Chan, C. Hahn, J. K. Nørskov, T. F. Jaramillo, and I. Chorkendorff, "Progress and perspectives of electrochemical CO_2 reduction on copper in aqueous electrolyte," Chem. Rev. **119**, 7610–7672 (2019).

[2] P. De Luna, C. Hahn, D. Higgins, S. A. Jaffer, T. F. Jaramillo, and E. H. Sargent, "What would it take for renewably powered electrosynthesis to displace petrochemical processes?," Science **364**, eaav3506 (2019).

[3] G. Wang, J. Chen, Y. Ding, P. Cai, L. Yi, Y. Li, C. Tu, Y. Hou, Z. Wen, and L. Dai, "Electrocatalysis for CO_2 conversion: From fundamentals to value-added products," Chem. Soc. Rev. **50**, 4993–5061 (2021).

[4] X. Tan, C. Yu, Y. Ren, S. Cui, W. Li, and J. Qiu, "Recent advances in innovative strategies for the CO_2 electroreduction reaction," Energy Environ. Sci. **14**, 765–780 (2021).

[5] J. Zhao, S. Xue, J. Barber, Y. Zhou, J. Meng, and X. Ke, "An overview of Cu-based heterogeneous electrocatalysts for CO_2 reduction," J. Mater. Chem. A **8**, 4700–4734 (2020).

[6] X. Li, X. Wu, X. Lv, J. Wang, and H. B. Wu, "Recent advances in metal-based electrocatalysts with hetero-interfaces for CO_2 reduction reaction," Chem. Catal. **2**, 262–291 (2022).

[7] L. Xie, Y. Jiang, W. Zhu, S. Ding, Y. Zhou, and J.-J. Zhu, "Cu-based catalyst designs in CO_2 electroreduction: Precise modulation of reaction intermediates for high-value chemical generation," Chem. Sci. **14**, 13629–13660 (2023).

[8] S. I. Allec, M.-T. Nguyen, R. Rousseau, and V.-A. Glezakou, "The role of subsurface hydrogen on CO_2 reduction and dynamics on Ni(110): An *ab initio* molecular dynamics study," J. Chem. Phys. **155**, 044702 (2021).

[9]T. Han, Y. Li, Y. Cao, I. Lee, X. Zhou, A. I. Frenkel, and F. Zaera, "*In situ* identification of surface sites in Cu–Pt bimetallic catalysts: Gas-induced metal segregation," J. Chem. Phys. **157**, 234706 (2022).
[10]Z.-Y. Du, K. Wang, Y.-M. Xie, Y. Zhao, Z.-X. Qian, S.-B. Li, Q.-N. Zheng, J.-H. Tian, A. V. Rudnev, Y.-J. Zhang, H. Zhang, and J.-F. Li, "*In situ* Raman reveals the critical role of Pd in electrocatalytic CO_2 reduction to CH_4 on Cu-based catalysts," J. Chem. Phys. **161**, 021101 (2024).
[11]W. Choi, H. Seong, V. Efremov, Y. Lee, S. Im, D.-H. Lim, J. S. Yoo, and D. Lee, "Controlled syngas production by electrocatalytic CO_2 reduction on formulated $Au_{25}(SR)_{18}$ and $PtAu_{24}(SR)_{18}$ nanoclusters," J. Chem. Phys. **155**, 014305 (2021).
[12]A. M. Ismail, G. F. Samu, H. C. Nguyën, E. Csapó, N. López, and C. Janáky, "Au/Pb interface allows the methane formation pathway in carbon dioxide electroreduction," ACS Catal. **10**, 5681–5690 (2020).
[13]X. Li, J. Wang, X. Lv, Y. Yang, Y. Xu, Q. Liu, and H. B. Wu, "Hetero-interfaces on Cu electrode for enhanced electrochemical conversion of CO_2 to multi-carbon products," Nano-Micro Lett. **14**, 134 (2022).
[14]P.-C. Chen, C. Chen, Y. Yang, A. L. Maulana, J. Jin, J. Feijoo, and P. Yang, "Chemical and structural evolution of AgCu catalysts in electrochemical CO_2 reduction," J. Am. Chem. Soc. **145**, 10116–10125 (2023).
[15]H. Nishi, Y. Zuo, Y. Kuroiwa, and T. Tatsuma, "Anisotropic growth of Au–Ag heteronanostructures through plasmon-induced reduction," J. Chem. Phys. **161**, 041101 (2024).
[16]C. Li, H. Xiong, M. He, B. Xu, and Q. Lu, "Oxyhydroxide species enhances CO_2 electroreduction to CO on Ag via coelectrolysis with O_2," ACS Catal. **11**, 12029–12037 (2021).
[17]S. Lee, G. Park, and J. Lee, "Importance of Ag–Cu biphasic boundaries for selective electrochemical reduction of CO_2 to ethanol," ACS Catal. **7**, 8594–8604 (2017).
[18]S. Back, J.-H. Kim, Y.-T. Kim, and Y. Jung, "Bifunctional interface of Au and Cu for improved CO_2 electroreduction," ACS Appl. Mater. Interfaces **8**, 23022–23027 (2016).
[19]C. Chen, X. Yan, S. Liu, Y. Wu, Q. Wan, X. Sun, Q. Zhu, H. Liu, J. Ma, L. Zheng, H. Wu, and B. Han, "Highly efficient electroreduction of CO_2 to C_{2+} alcohols on heterogeneous dual active sites," Angew. Chem., Int. Ed. **59**, 16459–16464 (2020).
[20]W. Zhang, Q. Qin, L. Dai, R. Qin, X. Zhao, X. Chen, D. Ou, J. Chen, T. T. Chuong, B. Wu, and N. Zheng, "Electrochemical reduction of carbon dioxide to methanol on hierarchical Pd/SnO_2 nanosheets with abundant Pd–O–Sn interfaces," Angew. Chem., Int. Ed. **57**, 9475–9479 (2018).
[21]W. Ma, S. Xie, T. Liu, Q. Fan, J. Ye, F. Sun, Z. Jiang, Q. Zhang, J. Cheng, and Y. Wang, "Electrocatalytic reduction of CO_2 to ethylene and ethanol through hydrogen-assisted C–C coupling over fluorine-modified copper," Nat. Catal. **3**, 478–487 (2020).
[22]S. Kuang, Y. Su, M. Li, H. Liu, H. Chuai, X. Chen, E. J. M. Hensen, T. J. Meyer, S. Zhang, and X. Ma, "Asymmetrical electrohydrogenation of CO_2 to ethanol with copper–gold heterojunctions," Proc. Natl. Acad. Sci. U. S. A. **120**, e2214175120 (2023).
[23]Y. C. Li, Z. Wang, T. Yuan, D. H. Nam, M. Luo, J. Wicks, B. Chen, J. Li, F. Li, F. P. G. de Arquer, Y. Wang, C. T. Dinh, O. Voznyy, D. Sinton, and E. H. Sargent, "Binding site diversity promotes CO_2 electroreduction to ethanol," J. Am. Chem. Soc. **141**, 8584–8591 (2019).
[24]J. Cai, Q. Zhao, W. Y. Hsu, C. Choi, Y. Liu, J. M. P. Martirez, C. Chen, J. Huang, E. A. Carter, and Y. Huang, "Highly selective electrochemical reduction of CO_2 into methane on nanotwinned Cu," J. Am. Chem. Soc. **145**, 9136–9143 (2023).
[25]X. Wang, P. Ou, J. Wicks, Y. Xie, Y. Wang, J. Li, J. Tam, D. Ren, J. Y. Howe, Z. Wang, A. Ozden, Y. Z. Finfrock, Y. Xu, Y. Li, A. S. Rasouli, K. Bertens, A. H. Ip, M. Graetzel, D. Sinton, and E. H. Sargent, "Gold-in-copper at low *CO coverage enables efficient electromethanation of CO_2," Nat. Commun. **12**, 3387 (2021).
[26]R. I. Masel, Z. Liu, H. Yang, J. J. Kaczur, D. Carrillo, S. Ren, D. Salvatore, and C. P. Berlinguette, "An industrial perspective on catalysts for low-temperature CO_2 electrolysis," Nat. Nanotechnol. **16**, 118–128 (2021).
[27]Y. Lum and J. W. Ager, "Sequential catalysis controls selectivity in electrochemical CO_2 reduction on Cu," Energy Environ. Sci. **11**, 2935–2944 (2018).
[28]G. O. Larrazábal, T. Shinagawa, A. J. Martín, and J. Pérez-Ramírez, "Microfabricated electrodes unravel the role of interfaces in multicomponent copper-based CO_2 reduction catalysts," Nat. Commun. **9**, 1477 (2018).
[29]W. J. Dong, J. W. Lim, D. M. Hong, J. Kim, J. Y. Park, W. S. Cho, S. Baek, and J. L. Lee, "Grain boundary engineering of Cu–Ag thin-film catalysts for selective (photo)electrochemical CO_2 reduction to CO and CH_4," ACS Appl. Mater. Interfaces **13**, 18905–18913 (2021).
[30]M. Michalak, A. Roguska, W. Nogala, and M. Opallo, "Patterning Cu nanostructures tailored for CO_2 reduction to electrooxidizable fuels and oxygen reduction in alkaline media," Nanoscale Adv. **1**, 2645–2653 (2019).
[31]J. K. Koh, Y. Jeon, Y. I. Cho, J. H. Kim, and Y.-G. Shul, "A facile preparation method of surface patterned polymer electrolyte membranes for fuel cell applications," J. Mater. Chem. A **2**, 8652–8659 (2014).
[32]Y. B. Kim, C.-M. Hsu, S. T. Connor, T. M. Gür, Y. Cui, and F. B. Prinz, "Nanopore patterned Pt array electrodes for triple phase boundary study in low temperature SOFC," J. Electrochem. Soc. **157**, B1269 (2010).
[33]F. L. P. Veenstra, A. J. Martín, and J. Pérez-Ramírez, "Nitride-derived copper modified with indium as a selective and highly stable catalyst for the electroreduction of carbon dioxide," ChemSusChem **12**, 3501–3508 (2019).
[34]Y. C. Li, Z. Yan, J. Hitt, R. Wycisk, P. N. Pintauro, and T. E. Mallouk, "Bipolar membranes inhibit product crossover in CO_2 electrolysis cells," Adv. Sustainable Syst. **2**, 1700187 (2018).
[35]S. Garg, C. A. Giron Rodriguez, T. E. Rufford, J. R. Varcoe, and B. Seger, "How membrane characteristics influence the performance of CO_2 and CO electrolysis," Energy Environ. Sci. **15**, 4440–4469 (2022).
[36]T. Zhang, J. C. Bui, Z. Li, A. T. Bell, A. Z. Weber, and J. Wu, "Highly selective and productive reduction of carbon dioxide to multicarbon products via in situ CO management using segmented tandem electrodes," Nat. Catal. **5**, 202 (2022).
[37]G. L. De Gregorio, T. Burdyny, A. Loiudice, P. Iyengar, W. A. Smith, and R. Buonsanti, "Facet-dependent selectivity of Cu catalysts in electrochemical CO_2 reduction at commercially viable current densities," ACS Catal. **10**, 4854–4862 (2020).
[38]Y. Yang, S. Louisia, S. Yu, J. Jin, I. Roh, C. Chen, M. V. Fonseca Guzman, J. Feijóo, P.-C. Chen, H. Wang, C. J. Pollock, X. Huang, Y.-T. Shao, C. Wang, D. A. Muller, H. D. Abruña, and P. Yang, "Operando studies reveal active Cu nanograins for CO_2 electroreduction," Nature **614**, 262–269 (2023).
[39]P. Wang, H. Yang, C. Tang, Y. Wu, Y. Zheng, T. Cheng, K. Davey, X. Huang, and S.-Z. Qiao, "Boosting electrocatalytic CO_2–to–ethanol production via asymmetric C–C coupling," Nat. Commun. **13**, 3754 (2022).
[40]H. Zhang, J. Gao, D. Raciti, and A. S. Hall, "Promoting Cu-catalysed CO_2 electroreduction to multicarbon products by tuning the activity of H_2O," Nat. Catal. **6**, 807–817 (2023).
[41]J. Li, I. Maresi, Y. Lum, and J. W. Ager, "Effects of surface diffusion in electrocatalytic CO_2 reduction on Cu revealed by kinetic Monte Carlo simulations," J. Chem. Phys. **155**, 164701 (2021).
[42]N. J. Harmon and H. Wang, "Electrochemical CO_2 reduction in the presence of impurities: Influences and mitigation strategies," Angew. Chem., Int. Ed. **61**, e202213782 (2022).
[43]C. Zhan, F. Dattila, C. Rettenmaier, A. Bergmann, S. Kühl, R. García-Muelas, N. López, and B. R. Cuenya, "Revealing the CO coverage-driven C–C coupling mechanism for electrochemical CO_2 reduction on Cu_2O nanocubes *via operando* Raman spectroscopy," ACS Catal. **11**, 7694–7701 (2021).
[44]H. Itahara, N. Sakamoto, T. Arai, N. Takahashi, S. Kosaka, and Y. Takatani, "Dealloyed intermetallic Cu_5Ca fine powders as nanoporous electrocatalysts for CO_2 reduction," ACS Appl. Nano Mater. **5**, 11991–11996 (2022).
[45]J. Wang, Z. Li, C. Dong, Y. Feng, J. Yang, H. Liu, and X. Du, "Silver/copper interface for relay electroreduction of carbon dioxide to ethylene," ACS Appl. Mater. Interfaces **11**, 2763–2767 (2019).
[46]R. Xie, Z. Hou, and G.-L. Chai, "Heusler alloy catalysts for electrochemical CO_2 reduction," J. Chem. Phys. **157**, 074704 (2022).
[47]J. Li, H. Xiong, X. Liu, D. Wu, D. Su, B. Xu, and Q. Lu, "Weak CO binding sites induced by Cu–Ag interfaces promote CO electroreduction to multi-carbon liquid products," Nat. Commun. **14**, 698 (2023).